Available online at www.sciencedirect.com
ScienceDirect
Solar Energy Materials & Solar Cells 91 (2007) 1726–1732
Solar Energy Materials and Solar Cells
www.elsevier.com/locate/solmat

Optical and structural properties of Ta_2O_5–CeO_2 thin films

D. Saygin-Hinczewski[a], K. Koc[a,b], I. Sorar[a], M. Hinczewski[c], F.Z. Tepehan[a], G.G. Tepehan[d,*]

[a]*Department of Physics, Istanbul Technical University, Maslak 34469, Istanbul, Turkey*
[b]*Department of Physics, Yildiz Technical University, Esenler 34220, Istanbul, Turkey*
[c]*Feza Gürsey Research Institute, TÜBİTAK–Bosphorus University, Çengelköy 34680, Istanbul, Turkey*
[d]*Faculty of Arts and Sciences, Kadir Has University, Cibali 34083, Istanbul, Turkey*

Received 3 December 2006; accepted 29 May 2007
Available online 16 July 2007

Abstract

In this study, the sol–gel spin-coating method has been used to make Ta_2O_5–CeO_2 thin films. These films have been prepared in various composition ratios to observe changes in their optical and structural properties. Reflectance and transmittance spectra were collected in the spectral range of 300–1000 nm and were accurately fit using the Tauc–Lorentz model. Film thicknesses, refractive indices, absorption coefficients, and optical band gaps were extracted from the theoretical fit. The highest refractive index value was found at 5% CeO_2 doping. The structure of the films was characterized by X-ray diffractometry and Fourier transform infrared spectrometry, while the surface morphology was examined through atomic force microscopy.

Keywords: Sol–gel; Spin coating; Ta_2O_5–CeO_2 thin films; Tauc–Lorentz model

1. Introduction

Ta_2O_5 films have been widely studied due to their chemical and thermal stability, high dielectric constant and refractive index. Their applications include ion conductors for electrochromic devices [1,2], optical waveguides [3,4] and protective coatings [5]. As microelectronics moves toward the nanoscale, SiO_2 will reach its practical limit due to direct tunneling currents at 1–2 nm thicknesses, and high-permittivity materials like Ta_2O_5 are possible replacements for SiO_2 in next-generation devices such as ultra-high-density dynamic random-access memories (DRAMs) [6,7].

It is known, for certain composites of Ta_2O_5–TiO_2, Ta_2O_5–Al_2O_3, and Ta_2O_5–ZrO_2 polycrystalline ceramics [8–10], that there is a significant increase in the dielectric constant compared to pure Ta_2O_5; this has stimulated research of doped thin films of Ta_2O_5 for use in microelectronics. Gan et al. [11] investigated the change in the dielectric constant of magnetron sputtered Ta_2O_5–TiO_2 films as a function of the composition. Cevro deposited Ta_2O_5–SiO_2 thin films by ion-beam sputtering using a single ion-beam gun and determined the optical properties as a function of the composition of the films [12]. Cappellani et al. characterized sol–gel-made Ta_2O_5 and Ta_2O_5–TiO_2 dielectric thin films [13]. Kaliwoh et al. studied the growth of Ta_2O_5–TiO_2 films using excimer lamps with photo-induced CVD [14] and sol–gel methods [15]. The present work reports on the optical and structural properties of sol–gel derived Ta_2O_5–CeO_2 thin films for compositions of 5%, 10%, and 15% CeO_2 (by volume) prepared with the spin-coating method.

2. Experimental procedure

The preparation of Ta_2O_5 coating solution is described elsewhere [16], with the only difference that in our case, the initial molarity of tantalum ethoxide in ethanol was 0.13 M. Cerium oxide solution was prepared using cerium ammonium nitrate ($Ce(NH_4)_2(NO_3)_6$) [99.99 + %, Aldrich], absolute ethyl alcohol (EtOH) [99.8%, Riedel-deHaën], nitric acid (HNO_3) [65%, Carlo] and diethanolamine (DEA,

*Corresponding author. Fax: +90 212 285 6386.
E-mail address: tepehan@khas.edu.tr (G.G. Tepehan).

0927-0248/$ - see front matter © 2007 Elsevier B.V. All rights reserved.
doi:10.1016/j.solmat.2007.05.029

(HOCHCH)NH) [99%, Aldrich]. DEA (0.4 ml), EtOH (20 ml) and nitric acid (0.02 ml) were first mixed together for 15 min through a magnetic stirrer. Then, cerium ammonium nitrate (1.8 g) was added. The complex solution was stirred for 1.5 h, and afterwards allowed to rest for 11 days, in which time the color of the final solution changed from red to pale yellow. The CeO_2 and freshly made Ta_2O_5 solutions were mixed at room temperature for 10 min in volume ratios of $(100-x)\%$ Ta_2O_5 to $x\%$ CeO_2, where $x = 0, 5, 10$, and 15.

Microscope slides (Corning 2947) were used as substrates. The glasses were first washed with a glass detergent, rinsed with water, then ultrasonically cleaned (Bandelin, Sonorex RK100, 35 kHz) for 15 min in ethanol. The solutions were spin coated on the substrates at 2000 rpm for 10 s. The films were preheat treated at 250 °C for 1 min in a microprocessor-controlled furnace (Carbolite, CWF 1100). The coating and heating procedures were repeated five times before the films were finally heat treated at 550 °C for 1 h, at a heating rate (beginning from 250 °C) and cooling-down rate of 3 °C/ min.

The transmittance and reflectance of the film-substrate system were obtained using an NKD System Spectrophotometer (Aquila Instruments) in the wavelength region of 300–1000 nm and at an incident angle of 30°. The data were fitted using the Tauc–Lorentz dielectric function, taking into consideration the contribution of the substrate in order to yield the optical properties of the film alone, as described in the next section. In this manner the film thickness, refractive index, absorption coefficient, and optical band gap were obtained. X-ray diffraction measurements were performed by a diffractometer (XRD, GBC-MMA) operated at 35 kV and 28 mA using CuK_α radiation. A Fourier transform reflectance spectrometer (FTIR, Spectrum One, with an ATR attachment, Perkin Elmer) was used for the detection of transmittance spectra of the films in the range 4000–650 cm^{-1} at normal incidence. The surface roughness of the films was characterized by an atomic force microscope (AFM, SPM-9500J3, Shimadzu) operating in the contact mode.

3. Theoretical model

We construct a simple theoretical model which can be used to extract the film refractive index $n_{\text{film}}(\lambda)$ and absorption coefficient $\alpha_{\text{film}}(\lambda)$ functions from the reflectance and transmittance spectra of the film-substrate system, adapting the approach of Ref. [17]. Fig. 1(a) shows schematically the passage of a light beam through the system. Since the thickness of the film, $d_{\text{film}} \sim 10^2$ nm, has the same order of magnitude as the wavelength of the incident light, the multiple reflected and transmitted beams as the light is passing through the film are nearly coherent. In contrast, the thickness of the substrate is $d_{\text{sub}} \sim 10^6$ nm, so that beams passing one or more times through the substrate are treated as incoherent. We identify three sets of reflection and transmission coefficients, shown in Figs. 1(b)–(d): r_1, t_1, for a beam passing through the film from the outside in; r_2, t_2, for a beam from within the substrate hitting its uncoated back surface; and r_3, t_3, for a beam passing through the film from the inside out. All these coefficients can be easily determined through the standard transfer matrix method [18], and expressed as functions of d_{film}, $n_{\text{film}}(\lambda)$, $\alpha_{\text{film}}(\lambda)$, and the substrate refractive index $n_{\text{sub}}(\lambda)$. The reflection and transmission coefficients for beams making multiple passes through the substrate are just products of the r_i and t_i, as shown in Fig. 1(a). Additionally, we took into consideration that every time the light passes from one side of the substrate to the other, its intensity is reduced by a factor $\delta_{\text{sub}}(\lambda) = \exp(-\alpha_{\text{sub}}(\lambda) d_{\text{sub}})$, where $\alpha_{\text{sub}}(\lambda)$ is the substrate absorption coefficient. Even a relatively small increase in $\alpha_{\text{sub}}(\lambda)$, for example in the near-UV region ($\lambda \lesssim 350$ nm), will result in a significant intensity loss because $d_{\text{sub}} \sim 10^6$ nm. Putting

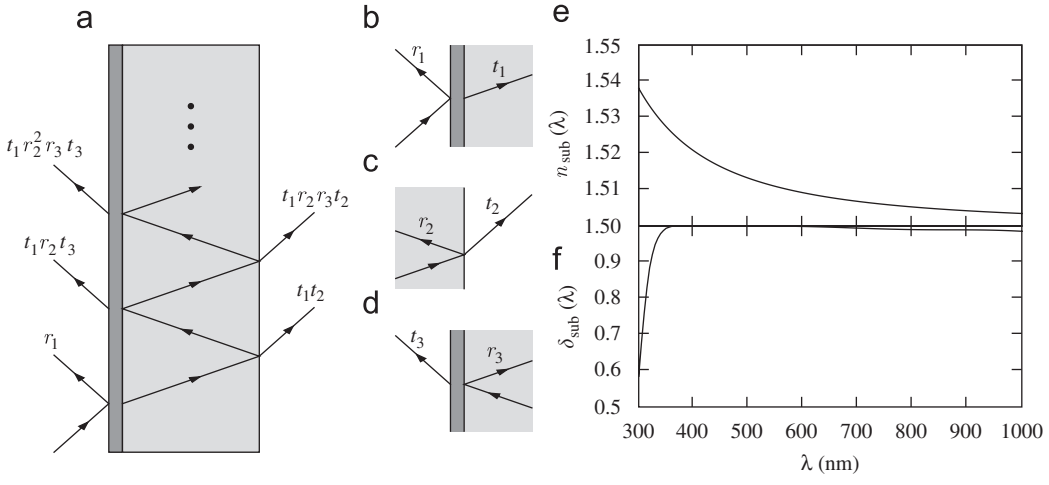

Fig. 1. (a) Schematic view of a light beam passing through the film (dark gray) and substrate (light gray) system, with the reflection coefficients contributing to the total R shown on the left, and the transmission coefficients contributing to the total T on the right. (b,c,d) The definition of the reflection and transmission coefficients $r_i, t_i, i = 1, \ldots, 3$, used in part (a) of the figure. (e) Index of refraction $n_{\text{sub}}(\lambda)$ for the Corning 2947 glass substrate as a function of wavelength λ. (f) Intensity attenuation factor $\delta_{\text{sub}}(\lambda) = \exp(-\alpha_{\text{sub}}(\lambda) d_{\text{sub}})$ for the substrate.

everything together, the total R and T of the film-substrate system is found by summing the coefficients of the series of beams incoherently:

$$R = |r_1|^2 + \sum_{n=0}^{\infty} \delta_{\text{sub}}^{2(n+1)} |t_1 r_2^{n+1} r_3^n t_3|^2 = |r_1|^2 + \frac{\delta_{\text{sub}}^2 |t_1 r_2 t_3|^2}{1 - \delta_{\text{sub}}^2 |r_2 r_3|^2}, \tag{1}$$

$$T = \sum_{n=0}^{\infty} \delta_{\text{sub}}^{2n+1} |t_1 r_2^n r_3^n t_2|^2 = \frac{\delta_{\text{sub}} |t_1 t_2|^2}{1 - \delta_{\text{sub}}^2 |r_2 r_3|^2}. \tag{2}$$

To determine $n_{\text{sub}}(\lambda)$ and $\delta_{\text{sub}}(\lambda)$, the reflectance and transmittance spectra of an uncoated substrate were fitted to a version of Eqs. (1) and (2) suitably modified for a naked substrate. This gives a value for $n_{\text{sub}}(\lambda)$ and $\delta_{\text{sub}}(\lambda)$ at each measured wavelength λ, and the values were interpolated to get continuous functions over the whole wavelength range. The results are shown in Fig. 1(e) and (f).

The final element of the theoretical description is the choice of a physical model for $n_{\text{film}}(\lambda)$ and $\alpha_{\text{film}}(\lambda)$. For this purpose we employed the Tauc–Lorentz form of the dielectric function [19], which has been successfully applied to a variety of semiconductors and insulators [20], among them thin layers of TiO_2, Ta_2O_5, and other optical coating materials [21]. In an attempt to capture the optical response of the material both near the optical band gap and at much larger energies, the imaginary part of the Tauc–Lorentz dielectric function was taken as the product of a Tauc law function and a Lorentz oscillator. In addition, the real and imaginary parts of the dielectric function were correctly related through a Kramers–Kronig transformation. As a result, the model was able to accurately reproduce experimental results over a wide spectral range, including regions both above and below the band edge. We used a modified version of the Tauc–Lorentz model which incorporates the possibility of Urbach tail absorption in the subgap region [22]. The imaginary part of the dielectric function $\varepsilon_2(E)$ as a function of photon energy E is given by

$$\varepsilon_2(E) = \begin{cases} \dfrac{E_1}{E} \exp\left(\dfrac{E - E_t}{E_u}\right) & \text{for } E \leqslant E_t, \\ \dfrac{A E_0 \Gamma (E - E_g)^2}{E\left[(E^2 - E_0^2)^2 + \Gamma^2 E^2\right]} & \text{for } E > E_t. \end{cases} \tag{3}$$

Here there are six fitting parameters with the dimension of energy, which are defined as follows: E_t marks the border between the region of Urbach tail and band-to-band transitions; E_g is the optical band gap; E_u controls the width of the Urbach tail, since the form of $\varepsilon_2(E)$ for $E \leqslant E_t$ leads to an absorption coefficient $\alpha_{\text{film}}(E) \propto \exp(E/E_u)$; A, E_0, and Γ are, respectively, the Lorentz oscillator amplitude, resonance energy, and oscillator width. The parameter E_1 is not free, but chosen so that ε_2 is continuous at $E = E_t$. In general, $E_t \geqslant E_g$, and the original Tauc–Lorentz model is obtained in the limit $E_u = 0$, $E_t = E_g$.

Table 1
Best-fit values for film thickness d_{film}, refractive index n_{film} at $\lambda = 550$ and 700 nm, and optical band gap E_g, obtained using the Tauc–Lorentz model in Eqs. (3)–(4)

Film	d_{film} (nm)	n_{film} (550 nm)	n_{film} (700 nm)	E_g (eV)
$x = 0$	210.8 ± 0.2	1.9465 ± 0.0012	1.9152 ± 0.0014	3.85 ± 0.06
$x = 5$	185.3 ± 0.2	2.012 ± 0.0017	1.9803 ± 0.0018	2.65 ± 0.02
$x = 10$	188.8 ± 0.2	1.9945 ± 0.0018	1.9604 ± 0.0019	2.62 ± 0.01
$x = 15$	190.7 ± 0.4	1.9701 ± 0.0036	1.9365 ± 0.0039	2.55 ± 0.03

Four films are shown, corresponding to solution volume ratios $(100 - x)\%$ Ta_2O_5–$x\%$ CeO_2, with $x = 0$, 5, 10, and 15.

The real part of the dielectric function $\varepsilon_1(E)$ is calculated through the Kramer–Kronig integral:

$$\varepsilon_1(E) = \varepsilon_{1\infty} + \frac{2}{\pi} P \int_0^{\infty} \mathrm{d}\xi \, \frac{\xi \varepsilon_2(\xi)}{\xi^2 - E^2}, \tag{4}$$

where the integration variable ξ runs over the entire energy range, P denotes the Cauchy principal value of the integral, and $\varepsilon_{1\infty}$ is an additional fitting parameter. Together with the film thickness d_{film}, this brings the total number of parameters to eight. However, this can be reduced to six by imposing two physical constraints [22], i.e. setting $\varepsilon_{1\infty} = 1$, and demanding that the slope of $\varepsilon_2(E)$ be continuous at $E = E_t$. The latter can be approximately satisfied by fixing $E_t = E_g + 2E_u$.

The index of refraction n_{film} and the absorption coefficient α_{film} are expressed in terms of ε_1 and ε_2 as

$$n_{\text{film}} = \left[\frac{(\varepsilon_1^2 + \varepsilon_2^2)^{1/2} + \varepsilon_1}{2}\right]^{1/2}, \tag{5}$$

$$\alpha_{\text{film}} = \frac{2E}{\hbar c}\left[\frac{(\varepsilon_1^2 + \varepsilon_2^2)^{1/2} - \varepsilon_1}{2}\right]^{1/2}. \tag{6}$$

Through the dependence of the r_i and t_i in Eqs. (1) and (2) on n_{film} and α_{film}, these optical functions can be directly used to calculate the reflectance R and transmittance T of the film-substrate system. Varying the six free parameters, we perform a least squares fit of the experimental R and T data using the Levenberg–Marquardt multivariate-regression algorithm (implemented by Wolfram Research's Mathematica software). Table 1 gives the results for the film thickness d_{film}, the optical band gap E_g, and the refractive index n_{film} at $\lambda = 550$ and 700 nm, along with the estimated uncertainties from the fitting. The best-fit of the R and T curves, with the corresponding n_{film} and α_{film}, are shown together with the experimental data in Fig. 2. It is clear that the Tauc–Lorentz model provides an excellent description of the system at all doping levels.

4. Results and discussion

Fig. 2 shows that the number of extrema in the R and T curves remains the same with increasing CeO_2 content for

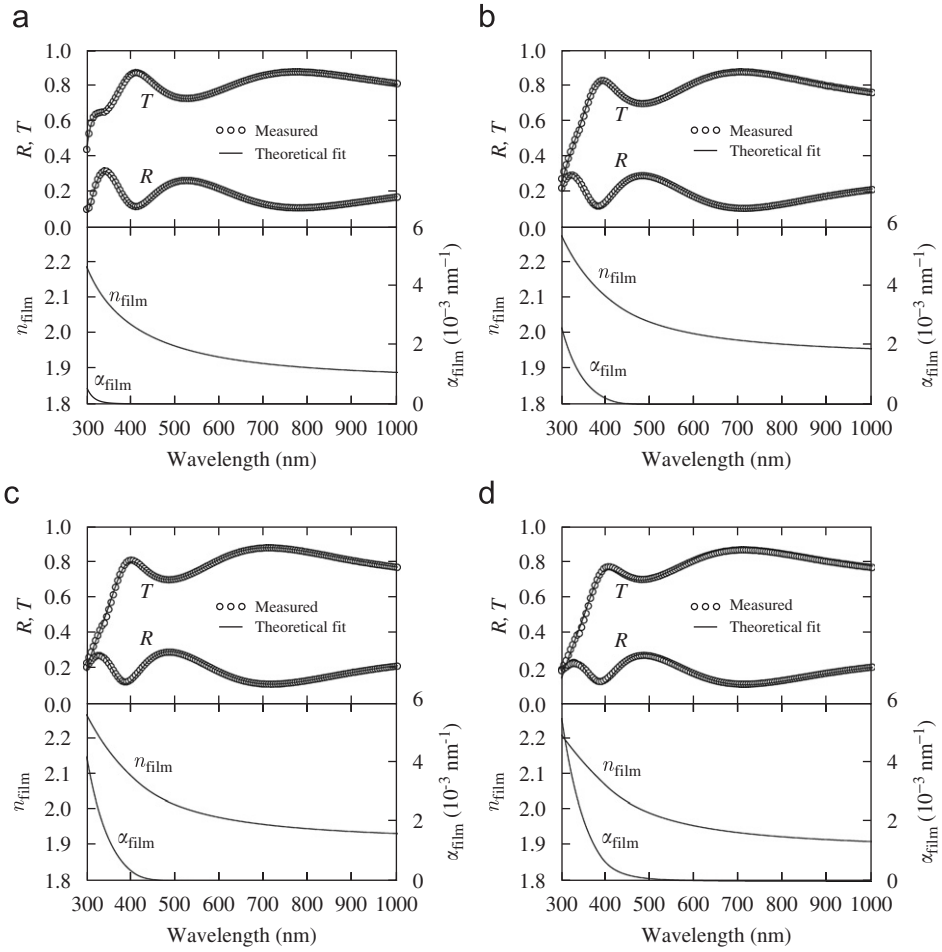

Fig. 2. Transmittance (T) and reflectance (R) spectra of Ta_2O_5–CeO_2 thin films coated on Corning 2947 substrates for different compositions, together with the best-fit Tauc–Lorentz curves for R, T, the film refractive index n_{film}, and the absorption coefficient α_{film}.

the given spectral region, which indicates that the film thicknesses are of the same order; this is supported by the thickness results in Table 1. For the visible region, the transmittance values are between 88–73% for the pure Ta_2O_5 film and 88–70% for the 5%, 10%, and 15% CeO_2-doped films. The maximum transmittance (88%) for the 100% Ta_2O_5 film is observed at the wavelength 780 nm; the 5%, 10%, and 15% CeO_2-doped films all have the maximum at 705 nm with values of 88%, 88% and 87%, respectively. The second-largest transmittance (87%) for the pure Ta_2O_5 film is reached at the wavelength 410 nm; the 5%, 10%, and 15% CeO_2-doped films have local maxima at 390, 400, 405 nm with values of 83%, 81% and 77%, respectively.

As evident from Table 1 and Fig. 3, there is a sudden increase in the refractive index when Ta_2O_5 is doped with 5% CeO_2. The index drops off at 10% doping (though the decrease is slight at shorter wavelengths), and again at 15%. The absorption coefficient in the near-UV region increases dramatically with CeO_2 doping, and the absorption edge shifts to longer wavelengths compared to the pure Ta_2O_5 film. This is reflected in the optical band gap, which shows a marked decrease from 3.85 ± 0.06 eV in the pure

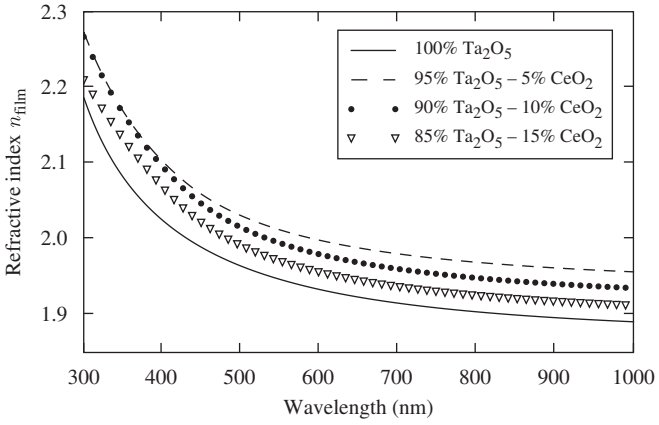

Fig. 3. Refractive index n_{film} of Ta_2O_5–CeO_2 thin films for different compositions.

sample (comparable to the earlier sol–gel result of 3.75 [16]) to 2.65 ± 0.02 eV at 5% doping. The band gap remains essentially unchanged (within the uncertainty) at 10% doping, but falls to 2.5 ± 0.03 eV at 15% doping.

The XRD measurements revealed that the Ta_2O_5–CeO_2 films heat treated at 550 °C were all amorphous. Even

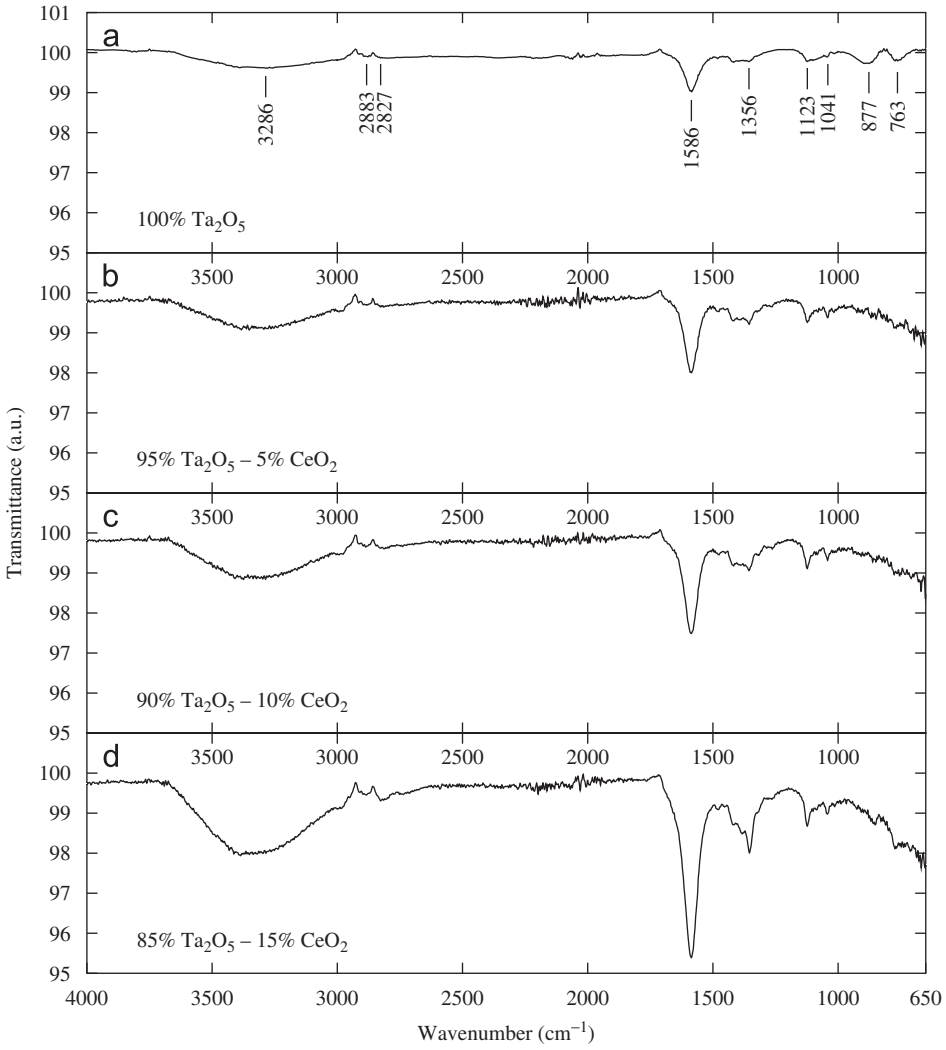

Fig. 4. ATR-FTIR spectra of Ta_2O_5–CeO_2 thin films for different compositions.

though CeO_2 has a crystallization temperature at or above 400 °C [23], because Ta_2O_5 begins to crystallize at 600 °C and becomes perfectly crystallized above 700 °C [24], Ta_2O_5 apparently shifted the crystallization temperature of CeO_2 to a higher value.

The evolution of the chemical structure of Ta_2O_5–CeO_2 thin films with the composition is given by the ATR-FTIR spectra in Fig. 4. In Fig. 4(a), Ta–O–Ta stretching vibrational modes can be seen between 650 and 800 cm^{-1}, while the 800–1000 cm^{-1} absorption band indicates the presence of suboxides TaO and TaO_2 [25]. The small bands located at 1041 and 1123 cm^{-1} belong to C–C and C–O bending modes, respectively. The band around 1356 cm^{-1} can be attributed to C–H deformation, which is supported by the stretching vibrational modes of C–H bonds found at 2827 and 2883 cm^{-1}. Similarly, vibrations of bending modes of C–H are seen in the sharp absorption peak at 1586 cm^{-1}, which is located in the 1498 − 1702 cm^{-1} band region [25,26]. The broad band around 3286 cm^{-1} is related to the stretching vibration of H_2O content and O–H groups. When Figs. 4(a)–(d) are compared, it can be seen that the Ta–O–Ta and TaO, TaO_2 suboxide absorption peaks and bands become less distinct with increasing CeO_2 concentration, while the amplitudes of the other absorption peaks increase.

AFM images of the Ta_2O_5–CeO_2 films are given in Fig. 5. The surface morphology is dominated by islands whose average diameters increase with doping: 79 ± 4, 97 ± 5, 107 ± 6, and 153 ± 8 nm going from the pure to the 15% doped samples. The maximum height ranges of the AFM images vary between 9 and 17 nm, indicating that even the steepest valleys between the islands are shallow compared to the total thickness of the films (≈ 200 nm). Thus the islands are connected to each other, at least within the resolution of the AFM probe. The root-mean-square (RMS) roughness values of the samples are 1.3, 1.8, 1.9, and 2.5 nm for the pure, 5%, 10%, and 15% CeO_2-doped films, respectively. These relatively small roughness values indicate that the top surfaces of the islands are nearly coplanar, with a slight increase in roughness at larger

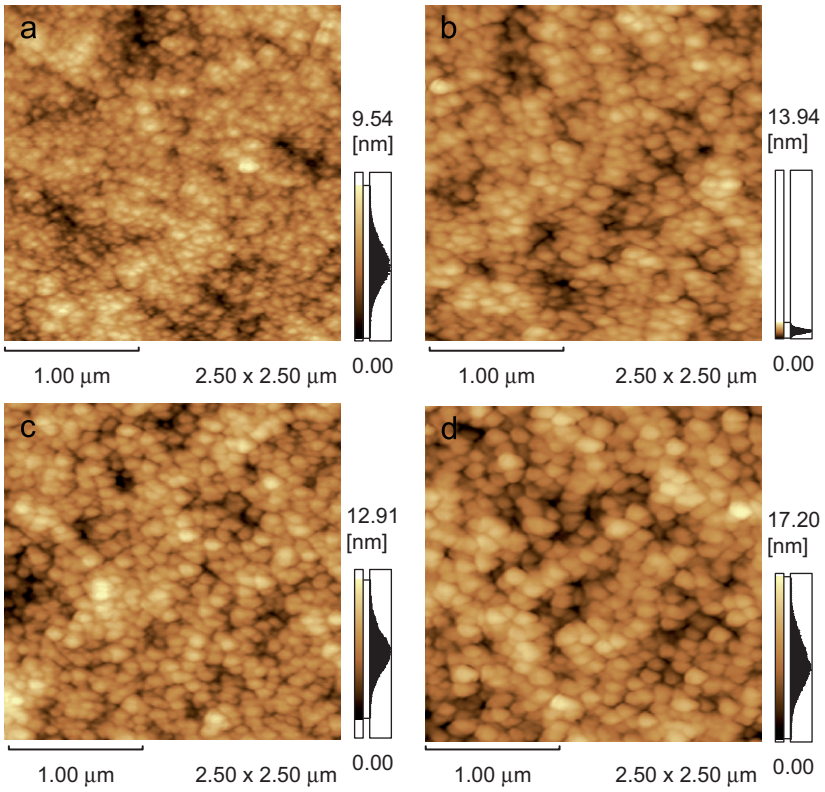

Fig. 5. AFM images of Ta_2O_5–CeO_2 thin films for different compositions, depicting areas of dimension 2.50 µm × 2.50 µm. The bar on the right of each image is a histogram showing the distribution of heights, with the total height range in nm indicated by the number above the bar. Zero height corresponds to the maximum depth reached by the AFM probe. (a) 100% Ta_2O_5, (b) 95% Ta_2O_5–5% CeO_2, (c) 90% Ta_2O_5–10% CeO_2, (d) 85% Ta_2O_5–15% CeO_2.

dopings. At all doping levels the films were found to be crack-free.

5. Conclusion

This work examined how the optical and structural properties of sol–gel spin coated Ta_2O_5–CeO_2 thin films heat treated at 550 °C evolved with CeO_2 concentration. As determined through fitting to the Tauc–Lorentz model, the most notable change in the optical properties occurred with 5% CeO_2 doping: a significant increase of the refractive index and a decrease of the optical band gap. Characterization of the films showed that their structure was amorphous at all doping levels, while both the chemical properties and surface morphology changed. The latter exhibited connected islands of increasing diameter with doping, while the overall surface roughness remained small.

Acknowledgments

The authors would like to thank F.C. Cebeci and I. Özçeşmeci for the ATR-FTIR measurements done at the Physical Chemistry Laboratory (Department of Chemistry, Istanbul Technical University). The Turkish State Planning Organization and the Research Fund of Istanbul Technical University have generously supported this research.

References

[1] N. Ozer, C.M. Lampert, J. Sol–Gel Sci. Technol. 8 (1997) 703.
[2] G. Frenning, F. Engelmark, G.A. Niklasson, M. Stromme, J. Electrochem. Soc. 148 (2001) A418.
[3] A.K. Chu, M.J. Chuang, IEEE Photonics Technol. Lett. 12 (2000) 1192.
[4] S. Kawakami, T. Sato, K. Miura, Y. Ohtera, T. Kawashima, H. Ohkubo, IEEE Photonics Technol. Lett. 15 (2003) 816.
[5] W.W. Albrecht, Production, properties, and application of tantalum, niobium and compounds, in: Lanthanides, Tantalum and Niobium, Springer, Berlin, 1989.
[6] E. Atanassova, A. Paskeleva, J. Mater Sci.: Mater. Electron. 14 (2003) 671.
[7] G.Q. Lo, D.L. Kwong, P.C. Fazan, V.K. Mathews, N. Sandler, IEEE Electron. Device Lett. 14 (1993) 216.
[8] R.F. Cava, W.F. Peck Jr., J.J. Krajewski, Nature 377 (1995) 215.
[9] R.J. Cava, W.F. Peck Jr., J.J. Krajewski, G.L. Roberts, B.P. Barber, H.M. O'Bryan, P.L. Gammel, Appl. Phys. Lett. 70 (1997) 1396.
[10] R.J. Cava, J.J. Krajewski, J. Appl. Phys. 83 (1998) 1613.
[11] J.-Y. Gan, Y.C. Chang, T.B. Wu, Appl. Phys. Lett. 72 (1998) 332.
[12] M. Cevro, Thin Solid Films 258 (1995) 91.
[13] A. Cappellani, J.L. Keddie, N.P. Barradas, S.M. Jackson, Solid State Electron. 43 (1999) 1095.
[14] N. Kaliwoh, J.-Y. Zhang, I.W. Boyd, Appl. Surf. Sci. 186 (2002) 246.
[15] N. Kaliwoh, J.-Y. Zhang, I.W. Boyd, Appl. Surf. Sci. 168 (2000) 13.
[16] F.Z. Tepehan, F.E. Ghodsi, N. Ozer, G.G. Tepehan, Sol. Energy Mater. Sol. Cells 59 (1999) 265.
[17] D. Saygin Hinczewski, M. Hinczewski, F.Z. Tepehan, G.G. Tepehan, Sol. Energy Mater. Sol. Cells 87 (2005) 181.
[18] F.L. Pedrotti, L.S. Pedrotti, Introduction to Optics, Prentice-Hall, London, 1993, pp. 392–396.
[19] G.E. Jellison Jr., F.A. Modine, Appl. Phys. Lett. 69 (1996) 371.

[20] H. Chen, W.Z. Shen, Eur. Phys. J B 43 (2005) 503.
[21] B. von Blanckenhagen, D. Tonova, J. Ullmann, Appl. Opt. 41 (2002) 3137.
[22] A.S. Ferlauto, G.M. Ferreira, J.M. Pearce, C.R. Wronski, R.W. Collins, X. Deng, G. Ganguly, J. Appl. Phys. 92 (2002) 2424.
[23] N. Ozer, Sol. Energy Mater. Sol. Cells 68 (2001) 391.
[24] Z.F. Zhu, F. Yu, Y. Man, Q. Tian, Y. He, N. Wu, J. Solid State Chem. 178 (2005) 224.
[25] J.-Y. Zhang, B. Lim, I.W. Boyd, Thin Solid Films 336 (1998) 340.
[26] J.H. Zhang, Y.Q. Yang, J.M. Shen, J.A. Wang, J. Mol. Catal. A-Chem. 237 (2005) 182.